Automotive Experiences
Vol. 5 No. 3 (2022) pp. 433-451
p-ISSN: 2615-6202 e-ISSN: 2615-6636

Research Paper

Experimental Evaluation of Cone Wedge Shape based Electronic Wedge Brake Mechanism in Vehicle Braking System

Sharil Izwan Haris[1,2], **Fauzi Ahmad**[1], **Mohd Hanif Che Hasan**[3], **Ahmad Kamal Mat Yamin**[1]

[1]Faculty of Mechanical Engineering, Universiti Teknikal Malaysia Melaka (UTeM), 76100 Hang Tuah Jaya, Melaka, Malaysia
[2]Kolej Kemahiran Tinggi MARA Masjid Tanah, Km 1, Persiaran Paya Lebar, Ramuan China Besar, 78 300 Masjid Tanah, Melaka, Malaysia
[3]Faculty of Electrical and Electronic Engineering Technology, Universiti Teknikal Malaysia Melaka (UTeM), 76100 Hang Tuah Jaya, Melaka, Malaysia

izwan.haris@mara.gov.my

https://doi.org/10.31603/ae.7112

Published by Automotive Laboratory of Universitas Muhammadiyah Magelang collaboration with Association of Indonesian Vocational Educators (AIVE)

Article Info
Submitted:
06/02/2022
Revised:
21/07/2022
Accepted:
23/07/2022
Online first:
06/07/2022

Abstract

The brake system is one of the most critical parts of a vehicle's technology for avoiding accidents. The ultimate focus of the braking system is to guarantee that adequate stopping force is available to stop the vehicle's longitudinal movement. Therefore, the ability of a brake system to stop a vehicle must be examined in terms of analyzing the brake system's performance and the implementation of the brake system on actual vehicles. This study offers a performance evaluation of the Electronic Wedge Brake based on the Cone Wedge Shape (CW-EWB) on the vehicle brake systems. The evaluation was carried out through dynamic assessments, namely sudden braking tests at constant speeds of 40, 60, and 90 km/h using the MATLAB Simulink software simulation method and an experimental study using hardware-in-loop simulation (HILS). In the simulation study, the performance of the vehicle brake system using CW-EWB was compared with the brake performance of the vehicle using the conventional hydraulic brake (CHB). The results showed that CW-EWB behaved similarly to the hydraulic brake in terms of required brake torque output but with a faster response time, i.e., between 0.5 – 1 s. The HILS experimental study was conducted to evaluate the performance of the CW-EWB on actual vehicles. This method confirmed the HILS results against the simulation results with a variable response time of less than 6%. Vehicle body speed, wheel speed, longitudinal tire slip, and stopping distance experienced by the vehicle were all evaluated. The study's findings show that the proposed CW-EWB is quite effective and sufficiently dependable to be used as a vehicle brake system, notably in Antilock Braking Systems.

Keywords: Performance evaluation; Cone wedge shape; Electronic wedge brake; HILS; Sudden braking test

1. Introduction

Automotive technology trends are now more concerned with the safety measures that are an inherent aspect of a modern automobile. Following that, active safety elements are intended to prevent accidents or to limit the number of inevitable accidents [1]. One of the active safety systems that is frequently increased with intricate changes is the brake system. The necessity for better brake systems has prompted a shift in system control from mechanical to electrical. As a result, Brake by Wire (BBW) is invented, which includes Electronic Hydraulic Brake (EHB), Electronic Pneumatic Brake (EPB), and Electronic Mechanical Brake (EMB). Later, the BBW system was improved based on the need to

produce high-torque brakes with faster response by using a 12 V power source, resulting in the development of the most recent braking system known as Electronic Wedge Brake (EWB) [2]. The EWB system is a non-hydraulic braking system. Consequently, issues such as brake fluid leaks and evaporation that were once common with hydraulic brakes can be avoided [3], [4]. In addition, the EWB system is easier to operate and has a more reliable system model than the EHB and EPB braking systems [5].

Although it is known that EWB can give an immediate braking effect with only 12 V power, it still needs to be tested for its performance on the vehicle's brake system. The ability of a brake system to provide a sufficient value of torque in stopping the vehicle ensures that the brake system is truly effective [6], [7]. The performance of the EWB system on vehicles braking system had been evaluated using simulation and experimental methods. Instead of simulation, some researchers evaluate the performance of this EWB by using software in the loop simulation (SILS) method [8]–[11]. The evaluation results show relatively effective performance but the data obtained still needs to be validated with data from actual testing. Due to these constraints, some researchers had done experimental testing on actual vehicles [12], [13] and mini trailers as an experimental medium [8], [14]. However, the results obtained from the experimental studieds were slightly mismatch with the theoretical expectation and show some response delay due to the malfunction of the system and the safety issues during experiment [8], [12]–[14]. Testing on real vehicles also poses a high safety risk and requires a fail safe system for support in the event of a system failure [15]. Some researchers developed test rigs or test benches to evaluate the effectiveness of EWB systems on vehicle brake systems [16]–[25]. However, the method can also not ultimately determine the brake effectiveness because the analysis parameters only focus on the EWB as the actuator.

These findings indicate that there is another step is needed before the experimental study in a real vehicle can be conducted. Recently, a new testing method namely hardware-in-the-loop-simulation (HILS) has been proposed to test a system that has a critical safety issue before being used in a real system. This well-known technique helps to reduce the cost to develop full experimental models and removing safety concerns [26]. Some successful experimental studies using HILS reported in [3], [5], [27]–[30] and stated that the system tested using HILS has higher confident level in representing the behavior of a real system.

Of that reason, in this study, a new EWB namely Cone Wedge Shape based Electronic Wedge Brake (CW-EWB) had been developed and tested as a vehicle braking system through simulation and experimentation using the Hardware in the Loops Simulation (HILS). To evaluate the level of capability and efficiency of the CW-EWB, a series of simulations have been conducted using Matlab Simulink Software by comparing the braking performance of vehicles using CW-EWB with the vehicles using conventional hydraulic brakes. While to assess the compatibility of the data between simulation and real, the HILS had been conducted with the aid of a test rig developed by including CW-EWB hardware in a loop that was coupled to a vehicle simulation model via sensing components and an input/output (I/O) device. The evaluation considers longitudinal tire slip, vehicle speed, wheel speed, and distance traveled of the vehicle.

This paper is organized as follows: The first section is the introductory section that provides the overview of the study. The second section describes the study's methodology including the CW-EWB design, the CW-EWB model, the CW-EWB control structure as well as the quarter vehicle traction model. The third section covers the results and discussion of vehicle model validation and performance evaluation of CW-EWBs in vehicle braking systems in both simulation and HILS, while the final section contains the conclusion.

2. Method

2.1. *The Electronic Wedge Brake Design*

Figure 1 depicts the design of the CW-EWB system, which includes the brake actuator and heart brake mechanism. The CW-EWB is powered by a direct current motor that is connected directly to the heart brake mechanism, which consists of a wedge mechanism, a calliper, and a brake pad connected by a lead screw (single style start). The lead screw is connected to the heart mechanism via a no-loss planetary reduction gear to provide

the required actuation force. The lead screw converts the angular motion of the DC motor to the axial motion of the brake wedge in the core. The details design of CW-EWB are stated in **Appendix 1**.

2.2. *The Electronic Wedge Brake Model*

Figure 2 depicts the body diagram of a CW-EWB wedge mechanism, which is based on [19]. Note that α is the wedges angle, F_m is the motor force, F_c is the clamping force between the disc and the brake pad, F_b is the stopping force generated from the relative motion between the pad and the disc surface and F_r is the wedge friction force that occurs between the upper and lower wedges. In this case, the angle of the driver screw β is set to be equal to α in order to amplify the force coming from the motor.

The actuator in this study was a permanent magnet direct current (PMDC) motor. Essentially, the PMDC motor is modelled by taking electrical and mechanical components into account. Here (J_m) is the inertia of the motor, (K_t) is the constant torque, (K_e) is the electromotive force constant, (D_m) is the viscous friction motor constant, and (T_l) is the load torque. Noting that (K_t) = (K_e) if there is no electromagnetic loss in the motor, the electrical power dissipated by the EMF back in the armature is directly converted to mechanical power.

The mathematical equations of the PMDC motor are shown as follows Eq. 1. For the armature circuits.

$$\dot{I}_m = -\frac{K_e}{L_m}\omega_m - \frac{R_m}{L_m}I_m + \frac{1}{L_m}V_m \tag{1}$$

By considering the mechanical load, the rotational acceleration of the DC motor shaft is described as Eq. 2:

$$\dot{\omega}_m = -\frac{D_m}{J_m}\omega_m + \frac{K_t}{J_m}I_m - \frac{1}{J_m}T_l \tag{2}$$

Here, a single lead screw-type start connects the PMDC motor directly to the brake mechanism. The required actuation force is then obtained by attaching the lead screw and a lossless planetary reduction gear to the heart mechanism.

Referring to **Figure 2**, the necessary motor drive force (F_m) can be calculated by considering several parameters of the lead screw such as the steadiness of the lead screw, (K_a), the viscous damping of lead screw, (D_a), the reduction of the lead screw gear ratio, (N_a) and the screw lead, (L_a). The lead screw plays an important role in turning the engine angle, (θ_m), engine speed (ω_m), and engine torque screw, (T_{screw}) into wedge position, (X_w), wedge speed, (V_w), and motor force, (F_m). Remember that when viewed from the motor side, the motor torque screw, (T_{screw}) is an engine load, (T_l).

The torque delivered to the screw can be represented by Eq. 3 and Eq. 4.

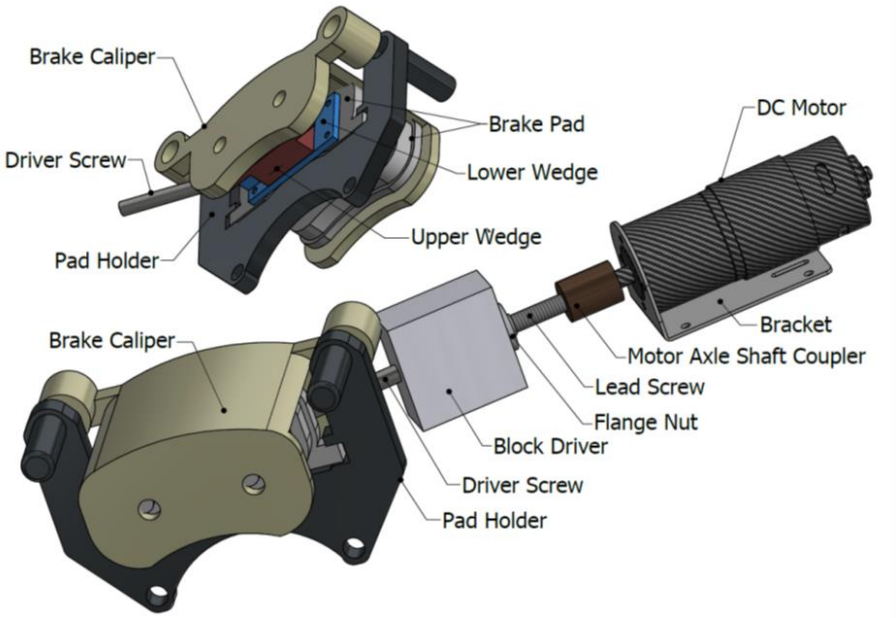

Figure 1. CW-EWB Design

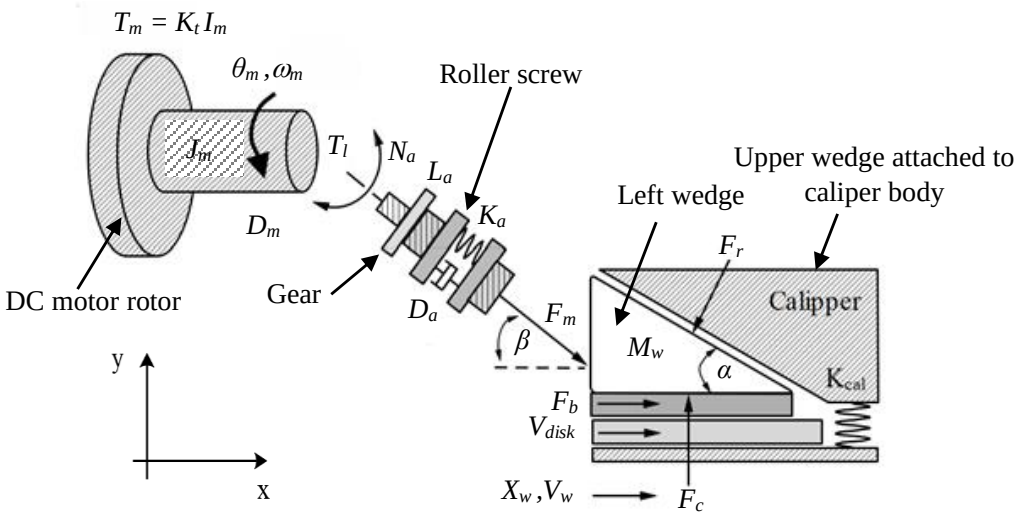

Figure 2. Basic body diagram of CW-EWB

$$T_{screw} = \frac{N_a L_a}{2\pi\eta}\left[K_a\left(L_a\frac{N_a\theta_m}{2\pi} - \frac{X_w}{\cos\beta}\right) + D_a\left(L_a\frac{N_a\dot{\theta_m}}{2\pi} - \frac{V_w}{\cos\beta}\right)\right] \quad (3)$$

$$F_m = 2\pi\eta\frac{T_{screw}}{N_a L_a} \quad (4)$$

By substituting (3) into (4), the motor force (Fm) can be defined as:

$$F_m = K_a\left(L_a\frac{N_a\theta_m}{2\pi} - \frac{X_w}{\cos\beta}\right) + D_a\left(L_a\frac{N_a\dot{\theta_m}}{2\pi} - \frac{V_w}{\cos\beta}\right) \quad (5)$$

as Equation (3), with the assumption that the planetary reduction gear mass is very light and the gear mechanism is less frictional. The lead screw output value ranges from 0 to 1. This is primarily determined by the geometry of the contact surfaces, their finishing, and the lead screw thread]s helix angle. It is also affected by operational factors such as load, speed, and lubrication. Although the efficiency of a lead screw is a true measured value, objective testing is the best way to determine the results. According to [13] and [24], the output of the lead screw used varies within a certain tolerance from its nominal value. As a result, the efficiency of the lead screw has been estimated to be 0.65 in this case.

Consider the CW-EWB with the angle of the motor shaft, β as in **Figure 2**, the relationship between the wedge actuation forces (F_m), reaction forces (F_r), and clamping forces (F_c) to the disc are derived based on force balance as follow:

The dynamic of a wedge in x-direction:

$$F_m\cos\beta + \mu F_c - F_r\sin\alpha = M_w\dot{V_w} \quad (6)$$

By dividing with tan α, yields,

$$F_r\cos\alpha = \frac{F_m\cos\beta + \mu F_c - M_w\dot{V_w}}{\tan\alpha} \quad (7)$$

Besides that, the dynamic of a wedge in y-direction can be stated as:

$$F_m\sin\beta + F_r\cos\alpha - F_c = M_w\dot{V_w}\tan\alpha \quad (8)$$

where M_w and V_w are wedge mass and wedge velocity in x-direction, respectively. Substituting equations (7) into (8), produces:

$$\dot{V_w} = \frac{F_n(\mu - \tan\alpha)}{M_w(\tan^2\alpha + 1)} + \frac{F_m(\sin\beta\tan\alpha + \cos\beta)}{M_w(\tan^2\alpha + 1)} \quad (9)$$

From equation (9), we want to simplify the complex multiplier formula of motor force (F_m), which is a function of the motor actuation angle and the wedge angle $f(\beta, \alpha)$. To maximise brake factor multiplication, the motor shaft angle should be the same as the wedge angle, rather than a zero angle as on a standard CW-EWB. Assuming the two angles are equal, this function can be summarised as follows Eq. 10.

$$f(\beta,\alpha) = \cos\beta + \sin\beta \tan\beta \tag{10}$$

thus,

$$f(\beta,\alpha) = \frac{1}{\cos\beta} \tag{11}$$

Thus, the simplified wedge dynamic model can be described as:

$$\dot{V}_w = \frac{1}{M_w(\tan^2\alpha + 1)}\left[F_c(\mu - \tan\alpha) + \frac{F_m}{\cos\beta}\right] \tag{12}$$

Meanwhile, the clamping force depends on the calliper stiffness (K_{cal}), wedge displacement, and wedge angle given by:

$$F_c = K_{cal} X_w \tan\alpha \tag{13}$$

Substitute (13) into (12) produces Eq. 14.

$$\dot{V}_w = \left[\frac{K_{cal}\tan\alpha\,(\mu - \tan\alpha)}{M_w(\tan^2\alpha + 1)}\right] X_w + \left[\frac{1}{M_w(\tan^2\alpha + 1)\cos\beta}\right] F_m \tag{14}$$

Table 1 lists the physical attributes used to evaluate the CW-EWB model, such as DC motors, brake pads, wedges, and etc. The **Appendix 2** contains the CW-EWB Simulink model.

2.3. *The EWB Control Structure*

Figure 3 depicts the torque tracking control of a CW-EWB, which is comprised of two primary controller loops namely torque control, which governs the entire output torque from the CW-EWB, and position control, which regulates the motor position in tracking the target torque. To obtain the appropriate response and to provide adequate tracking performance for the specified brake torque, a proportional-integral-derivative (PID) controller is employed in the torque control loop. While position control with the proportional-integral (PI) controller is used to adjust the position of the DC motor in order to keep a constant pad-to-disc brake gap distance. According to root locus depicted in **Figure 4**, the poles location were +47758i, -47758i, -9-6i, -9+6i, and 4 which located at the stable region. Here, the overshoot is limited to 30% with the fastest feasible reaction of rising time and settling time as well. The actuator input is monitored to avoid saturation which is limit to 12 V. Based on this

Table 1. The CW-EWB Parameters [31]

Parameter	Value
Motor Resistance, R_m	0.4781 Ω
Motor Inductance, L_m	0.0230 H
Electromotive Force Constant, K_e	0.0158 Nm/A
Torque constant, K_t	0.0156 Nm/A
Motor moment inertia, J_m	7.094 x 10^{-3} kgm²/s²
Motor viscous friction constant, D_m	1.9175e-5 Nms
Gear Reduction, N_a	1/24
Axial stiffness, K_a	750 x 10^6 N/m
Axial viscous friction constant, D_a	9.3279 x 10^{-05}
Roller Screw efficiency, η	0.63
Roller Screw Pitch, L_a	3e-3 m
Wedge Weight, M_w	0.3 kg
Wedge Angle, α	24.5 °
Motor axial angle, β	24.5 °
Calliper stiffness, K_{cal}	44.8385 x 10^6 N/m
Brake pad coefficient, μ	0.35

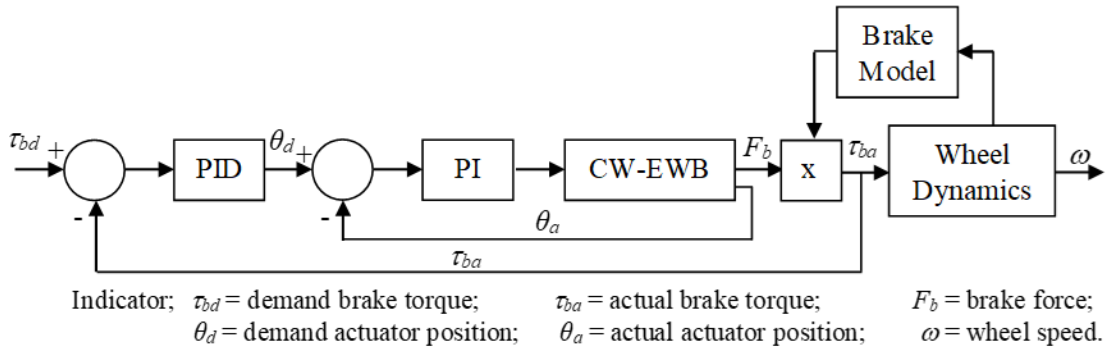

Figure 3. Control Structure of CW-EWB

consideration, the controller parameters shown in **Table 2** are established which are fine-tune using the Ziegler-Nichols approach.

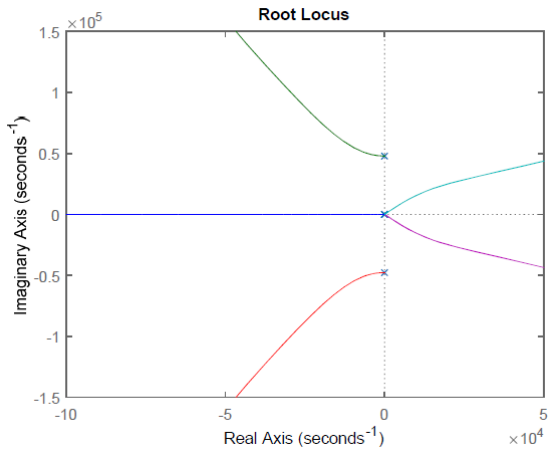

Figure 4. The root locus of the CW-EWB control structure

Table 2. Controller parameters

Controller	K_P	K_I	K_D
Position	0.000223	0.0005577	-
Torque	0.0002087	0.00068318	1.435×10^{-5}

2.4. *The Vehicle Models*

Figure 5 shows the vehicle model employed in this research, which is based on the two-degree-of-freedom (DOF) quarter vehicle traction model. The dynamics mathematical equations of the vehicle model can be derived from this figure, where m represents the quarter vehicle mass, v represents the vehicle velocity, F_x represents the tire longitudinal force, τ_w represents the wheel torque, τ_B represents the braking torque, F_z represents the normal force, and ω represents the wheel angular velocity. Several assumptions are established in the development of the vehicle model, which comprises of the longitudinal dynamics of the vehicle with a constant velocity v and the contact with the road represented by a wheel traction model. Other hypotheses include:

The vehicle model is made up of a single body (sprung mass) coupled to a wheel (unsprung mass). Aside from that, the vehicle was always planted, and the tyre never lost contact with the ground when maneuvring. The drag force produced by the vehicle during acceleration and braking is neglected in the simulation. Furthermore, the rolling resistance force is neglected because it is insignificant during braking.

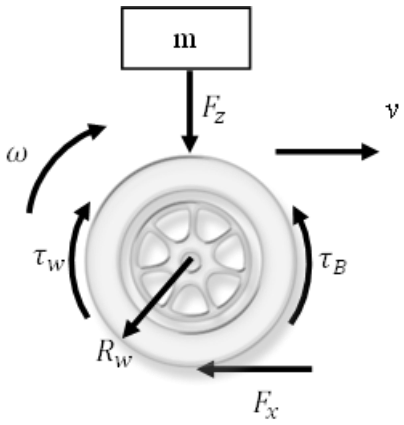

Figure 5. Quarter Vehicle Model

The simplified vehicle motion equation can be stated using Newton's second law as follows:

$$F_x = -m\dot{v} \tag{15}$$

The tyre friction force, F_x, can also be expressed as:

$$F_x = \mu F_z \tag{16}$$

where μ is the road adhesion coefficient the normal force, F_z may be expressed as:

$$F_z = -mg \tag{17}$$

where g is the gravitational mass.
By inserting Equation (15) and (16) into (17) and the equation (18) can be defined as:

$$\dot{v} = \mu g \tag{18}$$

During deceleration, braking torque is applied to the wheels, causing the wheel and vehicle to slow down. Simultaneously, the wheel rolling resistance force was ignored because it was insignificant in comparison to the friction force between the wheel and the road. Using Newton's second, the wheel motion equation can be expressed law as follows:

$$\tau_w - \tau_B = J_w \dot{\omega} \tag{19}$$

where J_w and $\dot{\omega}$ are wheel inertia and angular acceleration, respectively.
The wheel torque τ_w can be described as:

$$\tau_\omega = F_x R_w \tag{20}$$

where R_w denotes the wheel radius.

By inserting Equation (16), (17) and (19) into (20), equation (21) can be derived as:

$$\dot{\omega} = \frac{\mu m g R_w - \tau_B}{J_w} \tag{21}$$

Given that a vehicle travels at a constant speed, the wheel rotational velocity corresponds to the forward direction vehicle velocity. When the brake is applied, braking force is generated at the point of contact between the wheel and the road surface, resulting in a reduction in wheel speed. As the force on the wheel grows, there is slippage between the wheel and the road surface, which causes the wheel velocity to be less than the vehicle velocity [32]. Wheel slip, S, is defined as the difference in velocity during braking.

$$S = \frac{v - \omega R_w}{max(v/\omega R_w)} \tag{22}$$

2.5. *Hydraulic Brake Model*

The performance of the CW-EWB was evaluated by comparing the proposed brakes to the CHB. This evaluation employs the same methodology as as [3], [26], [34], in which the hydraulic brake is described as a first-order linear system with a pure time delay. All vacuum power aids, dynamic airflow, and static control valve mechanisms, as well as the modelling assumptions, are considered. The mathematical formulas for the model of hydraulic braking are available in [34] and [35].

A handling test method, which consisted primarily of straight-line braking, was conducted for validation. Experimentation should now be conducted under three speed limit conditions: 40 km/h for residential zones, 60 km/h for a federal highway, and 110 km/h for an interstate highway [36]. However, due to track restrictions, which have a maximum distance of about 200 m, the experimental validations were conducted at speeds of 40 km/h and 60 km/h, which correspond to the speed limits in residential zones and federal highways, respectively. This is due to the longer distance required to achieve and maintain a vehicle speed of more than 60 km/h. Another reason the 110 km/h speed validation test is not performed is the vehicle's limited capacity to produce a high-speed dynamic within the allowable distance. It should be noted that the vehicle features a 1300 cc engine, a five-speed manual gearbox, and a four-cylinder in-line engine.

3. Result and Discussion

This section addresses three sets of findings: vehicle model validation, CW-EWB braking performance through simulation research, and CW-EWB braking performance within the HILS environment. The validation of the vehicle model is used to evaluate the validity of the vehicle model by comparing the modelling performance to experimental data acquired from the actual vehicle. Simulation tests of vehicle braking using the CW-EWB are conducted in order to compare the performance of the brake system to that of a vehicle employing the CHB. In contrast, the HILS investigations are intended to test experimentally the performance of the CW-EWB hardware in delivering the needed brake torque to stop the vehicle in comparison to the simulation.

3.1. *Validation of Vehicle Model*

This section verifies the vehicle model using actual system measurements by comparing simulation results to experimental data from the vehicle [33]. In general, model validation entails determining how accurately the model and its accompanying data represent the actual vehicle system [37]. Nevertheless, the results from the vehicle model may not always correspond

precisely to the simulated responses, but they provide assurance that the model accurately represents the vehicle's behaviour.

Figure 6 depicts the model validation results for the 40 km/h brake test which includes speed comparison, tire longitudinal slip, stopping distance and brake torque. Based on the **Figure 6 (a)** the patterns of speeds between simulation results and experimental data are comparable, with minor deviations in transient responses accounting for a 4.6% discrepancy. At 2 s, the maximum braking force is applied, bringing the wheel to a complete stop at 2.49 and vehicle speed is fully stop at 3.63 s. The vehicle stops relatively late compared to the wheels due to the moment of inertia acting on the vehicle [38]. As seen in **Figure 6 (b)**, the difference in stopping time causes the wheel to drag on the road surface, resulting in slip to +1. This condition shows that the simulation can reproduce the behaviour of a real vehicle system in the transient state with a slight error of roughly 2.7%. The variance occurs because the driver cannot maintain a constant brake input during the experiment, unlike a simulation that assumes the brake input is always constant. The road profile of the test field having an uneven surface was also ignored by the simulations [3]. Despite minor variance in the previous conditions, the stopping distance response between the simulation and the experiment, as shown in **Figure 6 (c)**, was very close, with a similarity of up to 99%. The CHB model's ability to simulate a real CHB system by providing enough braking torque to stop the vehicle typically contributes to the excellent simulation performance that mimics the experimental response. **Figure 6 (d)** depicts the brake torque used in the simulation.

To further investigate the validity of the vehicle model, a brake test at a constant speed of 60 km/h was performed. **Figure 7 (a)** depicts the comparison of wheel and vehicle speeds between simulation and experiment data. The results indicate that the experimental data and simulation results correspond quite well, with only a 4% data discrepancy in the transient response. In contrast, as shown in **Figure 7 (b)**, the tire's longitudinal slip response showed a 2.7 % difference between simulations and experimental data, particularly between the intervals of 2.0 and 4.5 s. The validation results for the vehicle stopping distance are shown in **Figure 7 (c)**. The values obtained from simulations and experiments show a small deviation, with the experimental stopping distance only 0.18 m longer than the simulation distance. **Figure 7 (d)** shows the brake torque used by the simulation, which is 730 Nm.

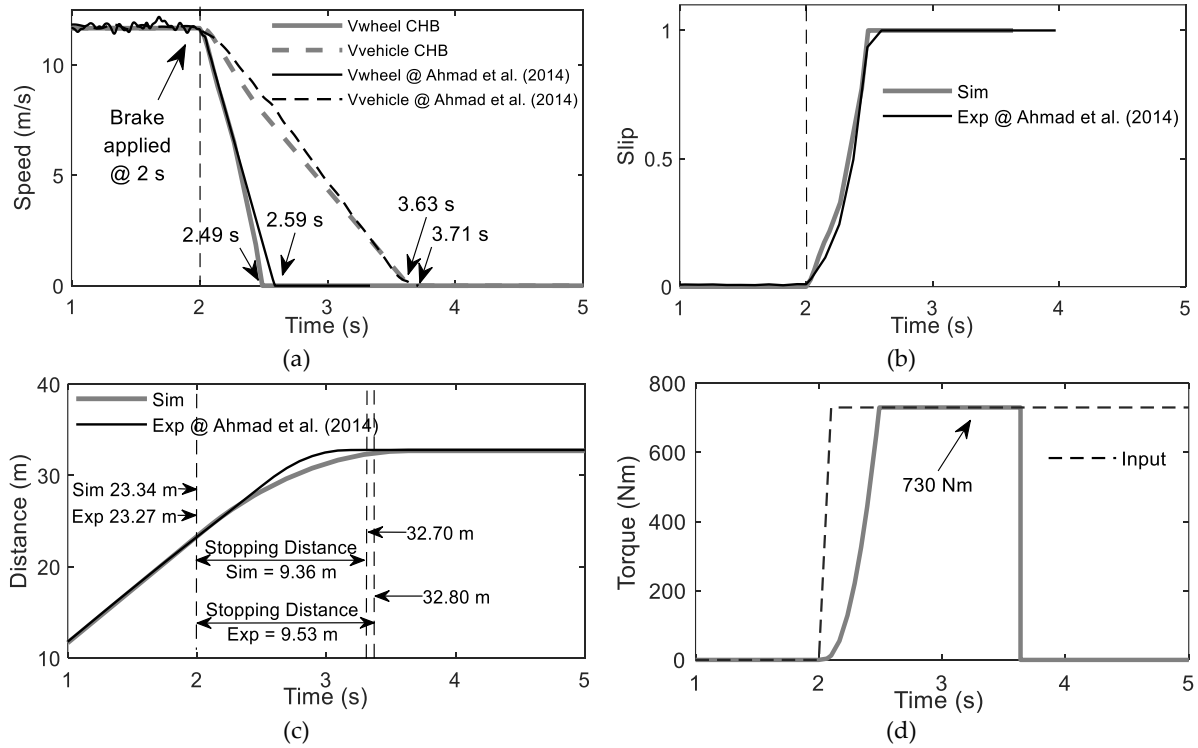

Figure 6. Validation results of the sudden braking test at 40 km/h constant speed; (a) Speed comparison; (b) Tire longitudinal slip; (c) Stopping distance; and (d) Brake torque

Based on the validation results, it can be concluded that the discrepancies between the simulation and experiment are due to the simplification and idealisation of the simulation model, as well as the driver's difficulty in maintaining the same desired speed as the simulation while manoeuvring. During the simulation's manoeuvre, it is also assumed that the vehicle travels on a level road. Uneven road profiles in the test field may also contribute to variance [33].

3.2. *Simulation Results of The Brake-Based CW-EWB*

Figure 8 shows the simulation framework for braking tests using EWB. There are two model blocks in this instance: the CW-EWB model and its torque monitoring controller, and the vehicle dynamic model. The brake torque demand (τ_d) is sent into the CW-EWB model, while the actual braking torque (τ_a) is fed into the vehicle dynamic model. In this study, the real tyre longitudinal slip (S), vehicle speed (V_v), wheel speed (V_w), and vehicle stopping distance (S_d) are evaluated using speeds at 40 km/h, 60 km/h, and 90 km/h. The brake torque input for braking testing is set to 730 Nm as same to vehicle validation stage.

Figure 9 illustrates the simulated outcomes of a CW-EWB based braking test conducted at 40 km/h. As presented in **Figure 9 (a)**, the CW-EWB achieves the desired braking torque with a faster rise time and settling time than the CHB. This caused the vehicle equipped with the CW-EWB to stop completely 0.30 s faster than the vehicle equipped with the CHB as shown in **Figure 9 (b)**. Monitoring the longitudinal slip reactions of the tyres is also used to determine braking performance alongside stopping time. As shown in **Figure 9 (c)**, the tyre longitudinal slip value of +1 indicates that the CW-EWB can give the vehicle the maximum braking torque required until the vehicle stops, which is faster than the vehicle with CHB. As a result, the stopping distance recorded by the vehicle equipped with the CW-EWB is 1.49 m shorter than the stopping distance recorded by the vehicle equipped with the CHB, as demonstrated in **Figure 9 (d)**.

Figure 10 shows the simulation results for the 60 km/h brake test. As shown in **Figure 10 (a)**, the CW-EWB theoretically behaves as expected in supplying the required braking torque at this speed, where the CW-EWB has a faster response time than the CHB. As a result, the vehicle can stop approximately 0.47 s faster than a vehicle

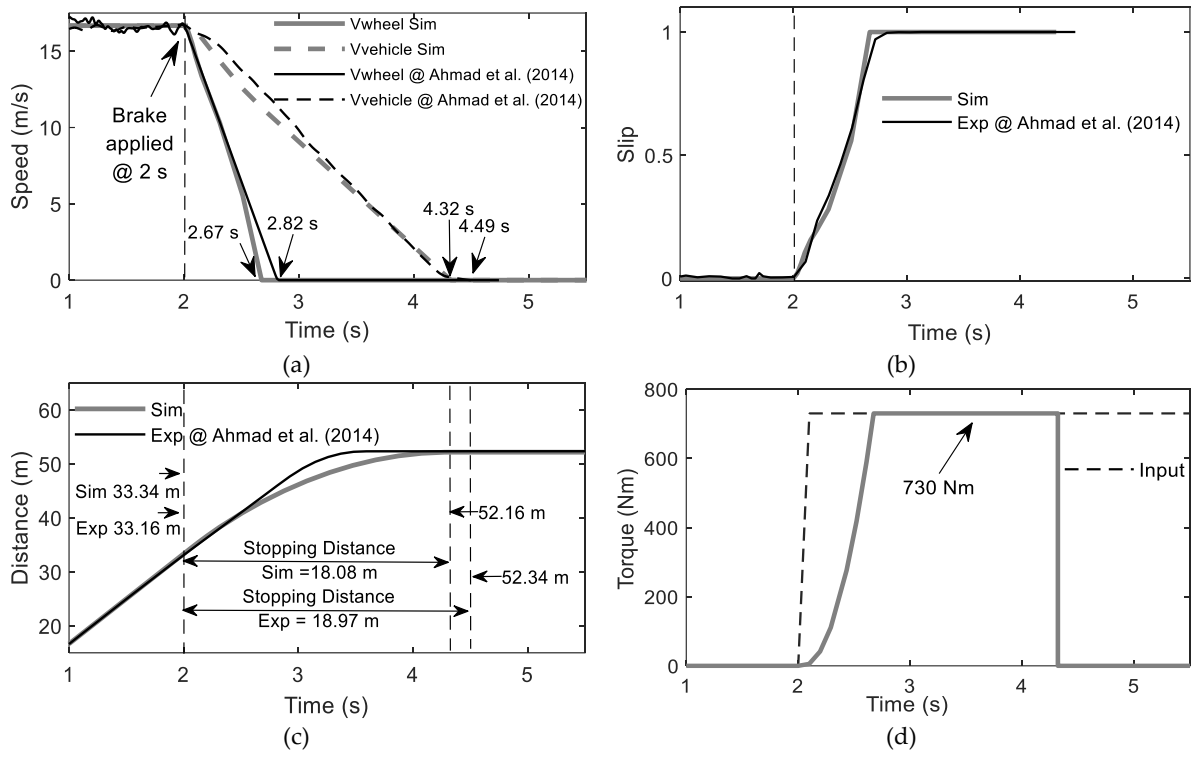

Figure 7. Validation results of the sudden braking test at 60 km/h constant speed; (a) Speed comparison; (b) Tire longitudinal slip; (c) Stopping distance; and (d) Brake torque.

equipped with a CHB, as shown in **Figure 10 (b)**, without sacrificing the ability to achieve maximum tire longitudinal slip in **Figure 10 (c)**. As illustrated in **Figure 10 (d)**, a vehicle equipped with a CW-EWB has a stopping distance of 2.99 m shorter than a vehicle equipped with a CHB.

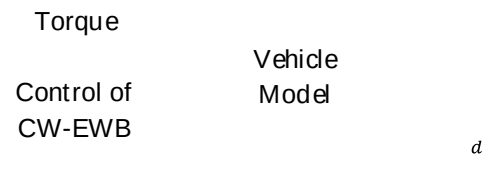

Figure 8. Framework for simulating braking tests with the CW-EWB

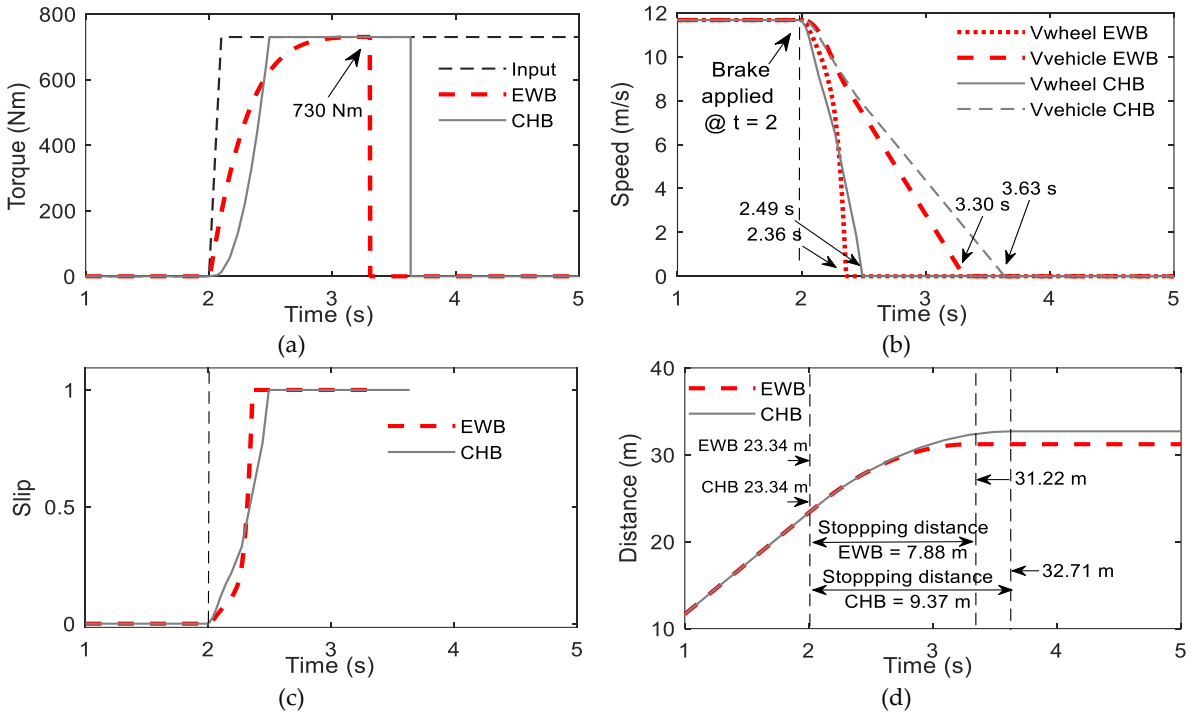

Figure 9. Braking test at 40 km/h using CW-EWB; (a) Brake torque; (b) Speed comparison; (c) Tyre longitudinal slip; and (d) Stopping distance

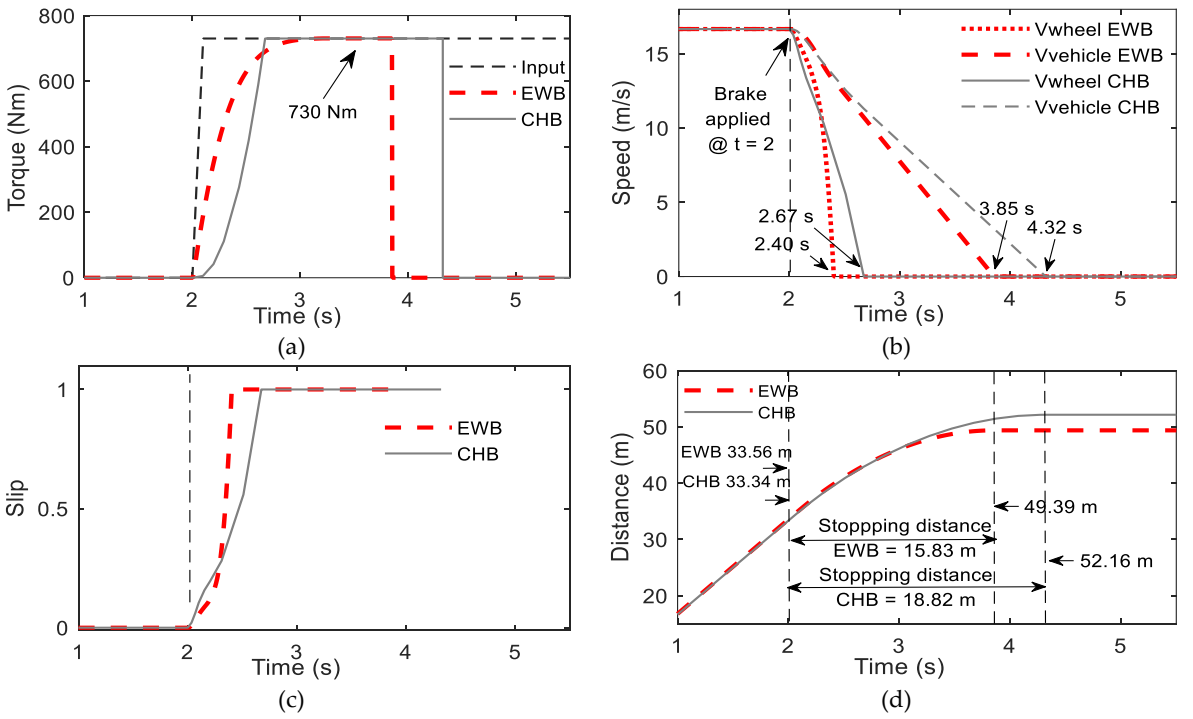

Figure 10. Braking test at 60 km/h using CW-EWB; (a) Brake torque; (b) Speed comparison; (c) Tyre longitudinal slip; (d) Stopping distance

The planned CW-EWB capacity in the vehicle's braking system is also evaluated in terms of the vehicle's maximum permitted speed maneuver on a federal highway, which is 90 km/h [36]. **Figure 11 (a)** shows that the applied braking torque enables the CW-EWB to stop a vehicle travelling at 90 km/h with excellent performance. It is capable of stopping a vehicle about 0.7 s faster than a CHB-equipped vehicle, where a CW-EWB-equipped vehicle stops completely after 4.76 seconds, while a CHB-equipped vehicle stops completely after 5.46 seconds, as illustrated in **Figure 11 (b)**. As a result, CW-EWB-equipped vehicles achieve maximum tire longitudinal slip faster than CHB-equipped vehicles, as shown in **Figure 11 (c)**. A significant reduction in stopping distance occurs in CW-EWB-equipped vehicles, up to 6.31 m less than the required stopping distance for a vehicle equipped with a CHB, as shown in **Figure 11 (d)**.

Based on the simulation comparison between CW-EWB and CHB vehicle brakes, it is possible to conclude that CW-EWB performs better than CHB, with a response time of 0.5–1 s faster. The results also show that the CW-EWB on the vehicle brake system can produce behaviour similar to the CHB brake system in braking torque production of around 730 Nm and achieve a +1 tyre longitudinal slip. The resulting distance is also approximately 15% shorter than CHB. In terms of performance, the CW-EWB demonstrates that it can be used to replace the CHB on vehicle brakes. This statement could be supported by a study on the potential of EWB by [39], which clearly shows that it has several advantages over conventional braking systems.

3.3. *HILS Results of The Brake-Based CW-EWB*

Figure 12 displays the basic HILS configuration for CW-EWB brake testing. It consists of a CW-EWB actuator, a data gathering device, a force sensor, a speed sensor, and a built-in encoder. As indicated in **Figure 12**, the vehicle is retained in simulation mode on the host PC, and the actual CW-EWB hardware is used as the brake actuator. Integrating the simulation with the CW-EWB hardware, I/O devices such as encoders, force sensors, speed sensors, and a National Instruments PCI 6221 DAQ card coupled with a National Instruments CB-68LP were used. In the simulation, the encoder detects the rotational input to the calliper transmitted via the driveshaft and provides feedback to the brake controller. This input contains data on angular position and angular velocity. The force sensor, attached to the brake calliper, is used to calculate the braking

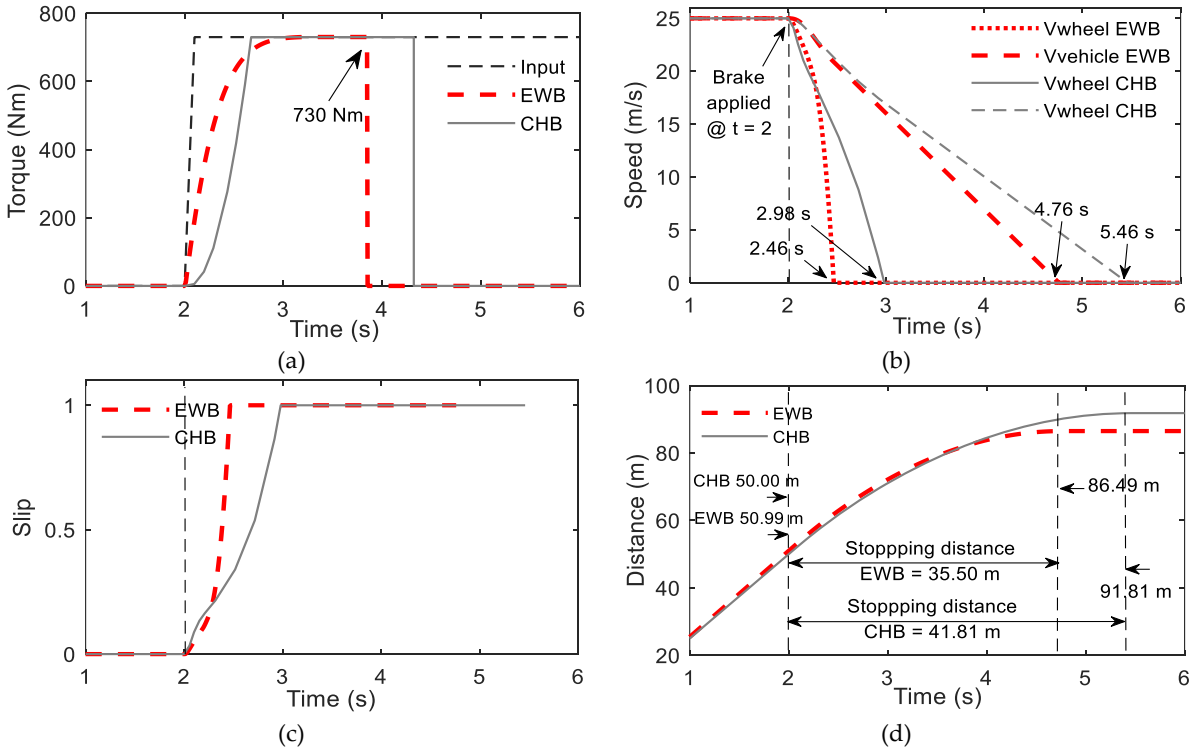

Figure 11. Braking test at 90 km/h using CW-EWB; (a) Brake torque; (b) Speed comparison; (c) Tyre longitudinal slip; (d) Stopping distance

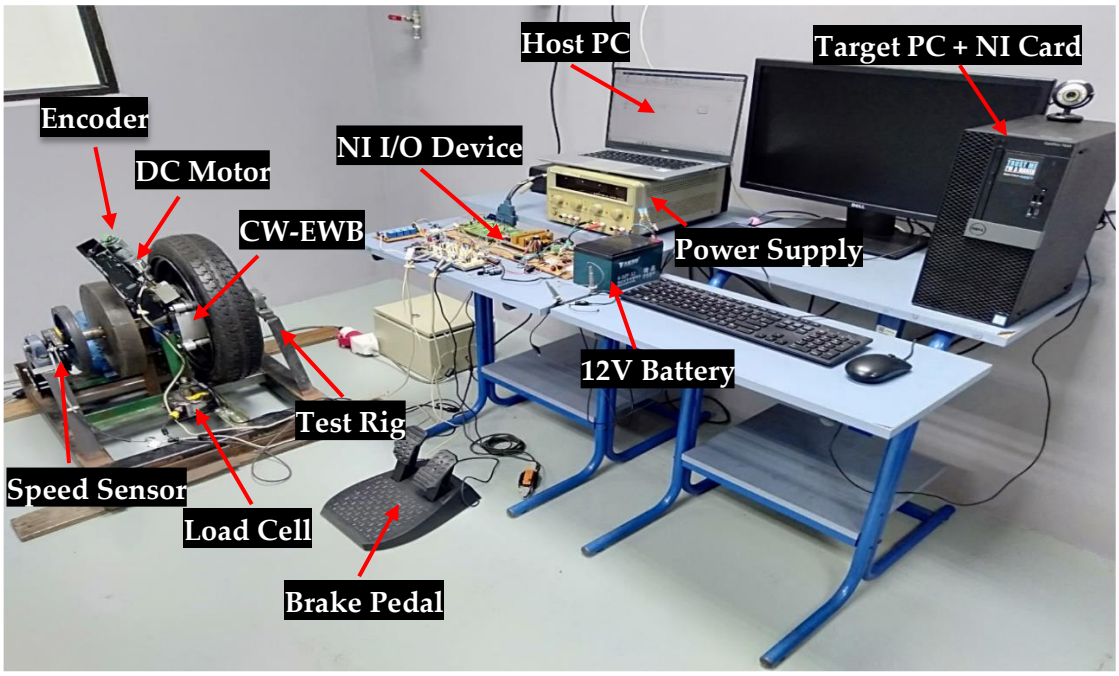

Figure 12. HILS Setup

torque created by the braking system and provide the brake input signal to the simulated vehicle through the National Instrument PCI 6221 DAQ. In contrast, the speed sensor is used to calculate the wheel speed.

Figure 13 shows the HILS brake test at 40 km/h using a CW-EWB actuator. The HILS pattern and the simulated response are quite similar but differ slightly in response time, where the HILS response is slower than the simulated response. **Figure 13 (a)** shows that the ability of the CW-EWB hardware to achieve the desired braking torque is 0.14 s slower than the simulation. As illustrated in **Figure 13 (b)**, the delay in braking torque generated

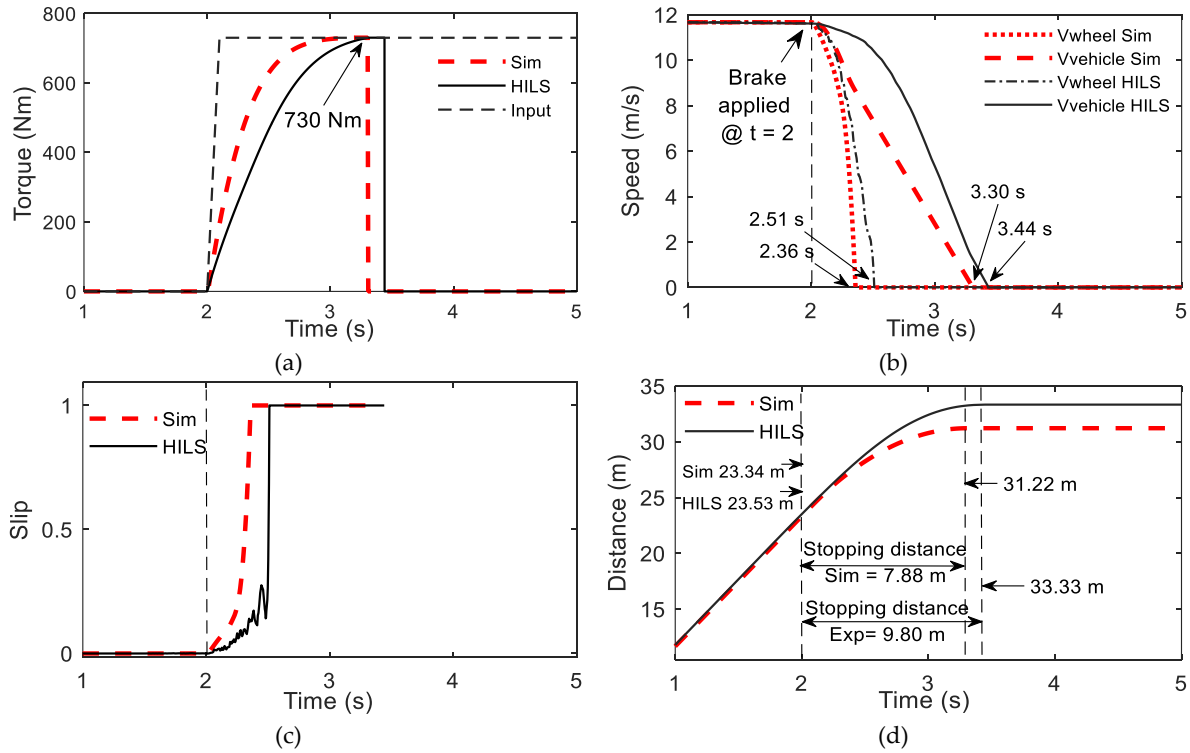

Figure 13. HILS braking test at 40 km/h using CW-EWB; (a) Brake torque; (b) Speed comparison; (c) Tyre longitudinal slip; and (d) Stopping distance

by the HILS has resulted in the ability of the HILS actuator to stop the vehicle more slowly than simulated. HILS requires 3.44 s to stop, while simulations require only 3.30 s. This condition has caused the HILS reaction to reach a +1 value for a relatively slower longitudinal slip than the simulation, as shown in **Figure 13 (c)**. At the same time, the HILS stop distance increased by 1.92 m compared to the simulation, as shown in **Figure 13 (d)**.

Figure 14 compares the HILS evaluation and simulation results for the 60 km/h braking test. Observations indicate variances between the simulation and HILS results for duration responses. This circumstance is again caused by the CW-EWB hardware's delay in generating the necessary input torque, as seen in **Figure 14 (a)**. As a result, the time required by the vehicle to stop using HILS is 4.00 s, compared to 3.85 s in simulation, as shown in **Figure 14 (b)**. The time required for the longitudinal slip of HILS to arrive at the +1 value is also slightly delayed compared to that shown by the simulation in **Figure 14 (c)**. As presented in **Figure 14 (d)**, the HILS stopping distance is 2.62 m longer than the simulation due to the delay in stopping time.

Figure 15 depicts the HILS findings of the braking test at a speed of 90 km/h. The trend between HILS and simulation data is comparable, with a slight divergence in the duration responses. As indicated in **Figure 15 (a)**, the delay in brake torque created by HILS to obtain the appropriate braking torque has resulted in HILS stopping time and distance being 0.16 s slower and 3.98 m longer than the simulation, as shown in **Figure 15 (b)** and **Figure 15 (d)**. The torque delay caused by the HILS reaction also causes a delay in reaching the +1 slip value compared to the simulation, as shown in **Figure 15 (c)**.

According to the results of the HILS test, the proposed CW-EWB system performs well in demonstrating its potential for use in actual vehicle applications. This condition is supported by the HILS performance results obtained in parallel with the simulations results. Although there was a difference in response time between HILS and the simulation, the difference was small and insignificant. The average delay of the HILS response compared to the simulated response was less than 6%. This shortcoming is caused by friction in the hardware system, particularly between two rough contact surfaces, as well as the inertia of the internal components of the DC motor, which slows the HILS system's response. The hardware finishing and DC motor limits can also contribute to slower system response [5], [40].

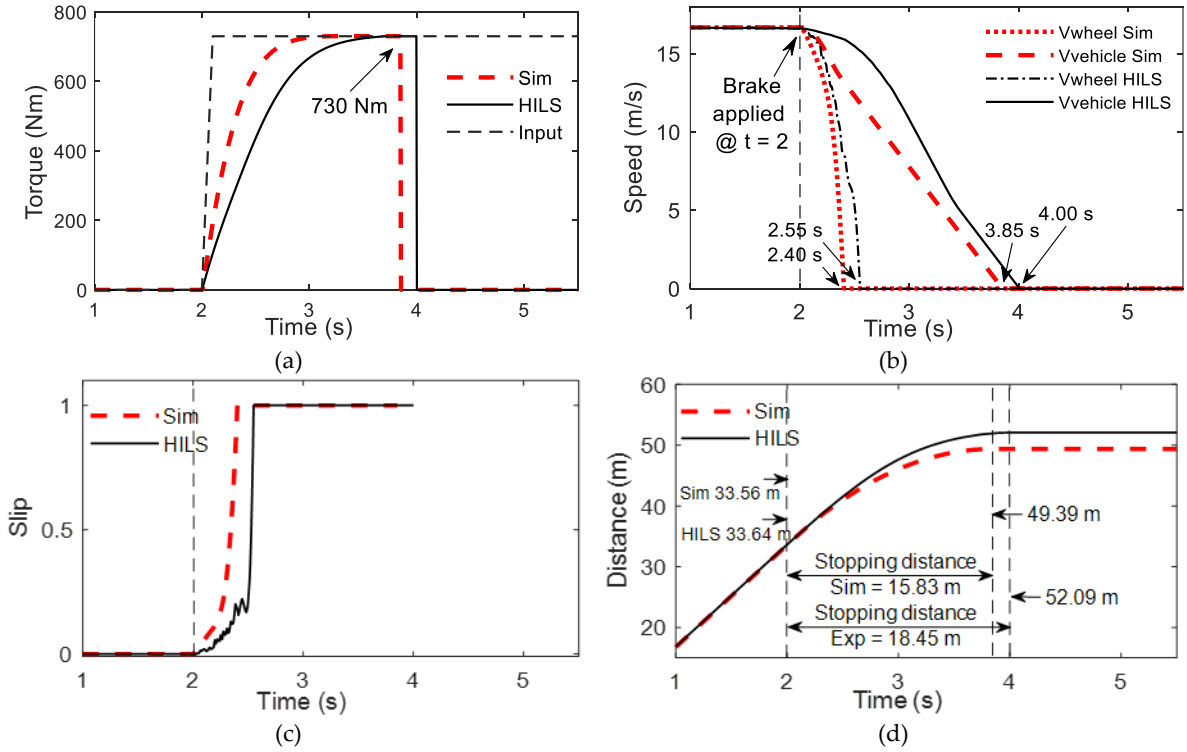

Figure 14. HILS braking test at 60 km/h using CW-EWB; (a) Brake torque; (b) Speed comparison; (c) Tyre longitudinal slip; and (d) Stopping distance

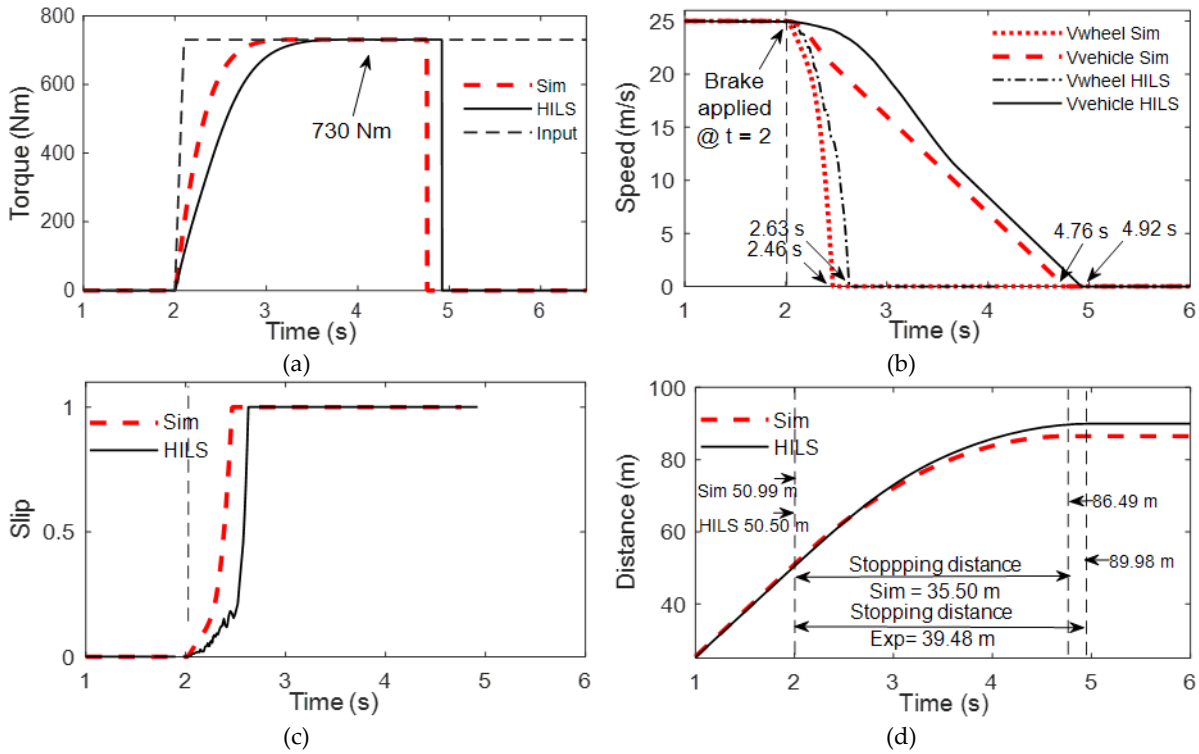

Figure 15. HILS braking test at 90 km/h using CW-EWB; (a) Brake torque; (b) Speed comparison; (c) Tyre longitudinal slip; and (d) Stopping distance

According to [38] and [41], the model response trend is the essential feature of a control-oriented model. The results can be accepted upon as long as the model response pattern is similar to the observed response with acceptable degrees of divergence and error. According to [42] and [43], the permissible variance between the observed response and the simulation is less than 10% of the time delay. Other researchers, such as [28], have argued that the permissible latency between simulations and experiments is less than 1 s. Furthermore, according to [44], the maximum error permitted to indicate the believability of a simulation is 10 %. Due to these facts, it is feasible to demonstrate the validity of HILS's results.

4. Conclusion

In this study, the CW-EWB performance evaluation on the vehicle brake system was conducted using a dynamic test known as the sudden braking test at constant speeds of 40, 60, and 90 km/h. The assessments were made through simulation methods and experimental HILS in evaluating various vehicle behaviours, including body and wheel speed, longitudinal tire slip, and vehicle travel distance. The simulation results show that CW-EWB on a vehicle brake system can produce similar behaviour to a CHB brake system, with a response time of around 0.5-1 s faster than CHB. The CW-EWB performance assessed through experimental HILS, in turn, showed satisfactory overall response, acceptable performance, and stability. The experimental results confirm the simulation results with slight variations in the reaction time of less than 6%. The delay in the reaction time is due to friction in the mechanical system, which is not taken into account during the simulation. Overall, the proposed CW-EWB is sufficiently accurate to be used in the future as a vehicle's braking system, particularly for anti-locking braking systems. For future research, any disturbances that affect the performance evaluation of the CW-EWB should be taken into account either in simulation studies or experimental studies to ensure that the braking system is truly effective.

Acknowledgement

The authors would like to thank Universiti Teknikal Malaysia Melaka (UTeM) for funding this work under an internal grant PJP/2020/FKM/PP/S01783.

Author's Declaration

Authors' contributions and responsibilities

The authors made substantial contributions to the conception and design of the study. The authors took responsibility for data analysis, interpretation and discussion of results. The authors read and approved the final manuscript.

Funding

This work is funded by the Universiti Teknikal Malaysia Melaka (UTeM) under an internal grant PJP/2020/FKM/PP/S01783.

Availability of data and materials

All data are available from the authors.

Competing interests

The authors declare no competing interest.

Additional information

No additional information from the authors.

References

[1] V. Dankan Gowda, A. C. Ramachandra, M. N. Thippeswamy, C. Pandurangappa, and P. Ramesh Naidu, "Modelling and performance evaluation of anti-lock braking system," *Journal of Engineering Science and Technology*, vol. 14, no. 5, pp. 3028–3045, 2019.

[2] M. H. Che Hasan, M. K. Hassan, and F. Ahmad, "Modelling and Simulation of Electronic Wedge Brake Based Antilock Brake System," *International Journal of Advanced Control and Automation System*, 2019.

[3] F. Ahmad, K. Hudha, S. A. Mazlan, H. Jamaluddin, V. R. Aparow, and M. R. M. Yunos, "Simulation and experimental investigation of vehicle braking system employing a fixed caliper based electronic wedge brake," *Simulation*, vol. 94, no. 4, pp. 327–340, 2018, doi: 10.1177/0037549717733805.

[4] M. L. H. Muhammad Luqman *et al.*, "Design and clamping force modelling of electronic wedge brake system for automotive application," *International Journal of Vehicle Systems Modelling and Testing*, vol. 8, no. 2, pp. 145–156, 2013, doi: 10.1504/IJVSMT.2013.054478.

[5] F. Ahmad *et al.*, "Modelling and control of a fixed calliper-based electronic wedge brake," *Strojniski Vestnik/Journal of Mechanical Engineering*, vol. 63, no. 3, pp. 181–190, 2017, doi: 10.5545/sv-jme.2016.3508.

[6] W. Batayneh, M. Jaradat, and A. Bataineh, "Intelligent adaptive control for anti-lock braking system," in *ASME International Mechanical Engineering Congress and Exposition, Proceedings (IMECE)*, 2018, vol. 4A-2018, pp. 1–13, doi: 10.1115/IMECE2018-87659.

[7] S. I. Haris, F. Ahmad, A. K. M. Yamin, and A. Saad, "Review on the design structure and research implemented on electronic wedge brake."

[8] Á. Semsey and R. Roberts, "Simulation in the development of the Electronic Wedge Brake," *SAE Technical Papers*, vol. 1, no. 724, 2006, doi: 10.4271/2006-01-0298.

[9] V. R. R. Aparow, K. Hudha, F. Ahmad, and H. Jamaluddin, "Development of Antilock Braking System Using Electronic Wedge Brake Model," *Journal of Mechanical Engineering and Technology*, vol. 6, no. 1, pp. 37–64, 2014.

[10] K. Han, K. Huh, J. Chun, M. Kim, and J. Kim, "Design Of Hardware Architecture And Control Algorithm For The Electronic Wedge Brake," in *Proceedings of the ASME 2010 Dynamic Systems and Control Conference DSCC2010*, 2010, pp. 1–6, doi: 10.1115/DSCC2010-4115.

[11] V. A. Ivanov, "Adjustable Electromechanical Wedge Brakes With Reduced Energy Consumption," *Proceedings of the ASME 2011 International Mechanical Engineering Congress & Exposition IMECE2011 November 11-17, 2011, Denver, Colorado, USA*, pp. 1–8, 2015, doi: 10.1115/IMECE2011-62915.

[12] J. G. Kim, M. J. Kim, J. H. Chun, and K. Huh, "ABS / ESC / EPB Control of Electronic Wedge Brake," *SAE Technical Papers*, pp. 2010-01–0074, 2012, doi: 10.4271/2010-01-0074.

[13] J. S. Cheon, "Brake by wire system configuration and functions using front EWB (Electric Wedge Brake) and rear EMB (Electro-Mechanical Brake) actuators," *SAE Technical Papers*, vol. 1, 2010, doi: 10.4271/2010-01-1708.

[14] L. M. Ho, R. Roberts, H. Hartmann, and B. Gombert, "The electronic wedge brake-EWB," 2006, doi: 10.4271/2006-01-3196.

[15] W. Li, Q. Zhang, and Y. Zhang, "The Effect of

ADRC on Vehicle Braking Performance," *Journal of Electrical Engineering and Technology*, vol. 15, no. 2, pp. 705–712, 2020, doi: 10.1007/s42835-019-00340-5.

[16] M. A. A. Emam, A. S. Emam, S. M. El-Demerdash, S. M. Shaban, and M. A. Mahmoud, "Performance of Automotive Self Reinforcement Brake System," *Journal of Mechanical Engineering*, vol. 1, no. 1, pp. 4–10, 2012.

[17] J. Fox, R. Roberts, C. Baier-Welt, L. M. Ho, L. Lacraru, and B. Gombert, "Modeling and Control of a Single Motor Electronic Wedge Brake," *SAE Technical Paper*, pp. 2007-01–0866, 2007, doi: 10.4271/2007-01-0866.

[18] N. M. Ghazaly, "A Preliminary Experimental Investigation of a New Wedge Disc Brake," *Int. Journal of Engineering Research and Applications*, vol. 3, no. 6, pp. 735–744, 2013.

[19] H. Hartmann, M. Schautt, A. Pascucci, and B. Gombert, "eBrake® - The Mechatronic Wedge Brake," *SAE Technical Paper Series*, vol. 1, no. 724, 2010, doi: 10.4271/2002-01-2582.

[20] C. H. Jo *et al.*, "Design and control of an upper-wedge-type electronic brake," *Proceedings of the Institution of Mechanical Engineers, Part D: Journal of Automobile Engineering*, vol. 224, no. 11, pp. 1393–1405, 2010, doi: 10.1243/09544070JAUTO1268.

[21] J. G. Kim, M. J. Kim, J. K. Kim, and K. H. Noh, "Developing of Electronic Wedge Brake with Cross Wedge," *SAE Technical Paper*, pp. 2009-01–0856, 2009, doi: 10.4271/2009-01-0856.

[22] H. Park and S. B. Choi, "Development of a sensorless control method for a self-energizing brake system using noncircular gears," *IEEE Transactions on Control Systems Technology*, vol. 21, no. 4, pp. 1328–1339, 2013, doi: 10.1109/TCST.2012.2204750.

[23] M. H. Putz, "VE mechatronic brake: Development and investigations of a simple electro mechanical brake," *SAE Technical Papers*, 2010, doi: 10.4271/2010-01-1682.

[24] R. Roberts, M. Schautt, H. Hartmann, and B. Gombert, "Modelling and Validation of the Mechatronic Wedge Brake," *SAE International*, 2003, doi: 10.4271/2003-01-3331.

[25] L. Yu, L. Ma, J. Song, and X. Liu, "Magnetorheological and Wedge Mechanism-Based Brake-by-Wire System with Self-Energizing and Self-Powered Capability by Brake Energy Harvesting," *IEEE/ASME Transactions on Mechatronics*, vol. 21, no. 5, pp. 2568–2580, 2016, doi: 10.1109/TMECH.2015.2512579.

[26] V. R. Aparow, K. Hudha, F. Ahmad, and H. Jamaluddin, "Modeling and validation of electronic wedge brake mechanism for vehicle safety system," *Jurnal Teknologi*, vol. 75, no. 1, pp. 183–191, 2015, doi: 10.11113/jt.v75.5286.

[27] F. Ahmad, S. A. Mazlan, H. Zamzuri, K. Hudha, and H. Jamaluddin, "Study on the potential application of electronic wedge brake for vehicle brake system," *International Journal of Modelling, Identification and Control*, vol. 23, no. 4, p. 306, 2015, doi: 10.1504/IJMIC.2015.070650.

[28] V. R. Aparow, K. Hudha, F. Ahmad, and H. Jamaluddin, "Model-in-the-loop simulation of gap and torque tracking control using electronic wedge brake actuator," *International Journal of Vehicle Safety*, vol. 7, no. 3–4, pp. 390–408, 2014, doi: 10.1504/IJVS.2014.063250.

[29] R. Roberts *et al.*, "Testing the mechatronic wedge brake," *SAE Technical Papers*, vol. 1, no. 724, pp. 2004-01–2766, 2004, doi: 10.4271/2004-01-2766.

[30] K. Han, M. Kim, and K. Huh, "Modeling and control of an electronic wedge brake," *Proceedings of the Institution of Mechanical Engineers, Part C: Journal of Mechanical Engineering Science*, vol. 226, no. 10, pp. 2440–2455, 2012, doi: 10.1177/0954406211435584.

[31] M. H. Che Hasan, M. Khair Hassan, F. Ahmad, and M. H. Marhaban, "Modelling and Design of Optimized Electronic Wedge Brake," in *2019 IEEE International Conference on Automatic Control and Intelligent Systems, I2CACIS 2019 - Proceedings*, 2019, no. June, pp. 189–193, doi: 10.1109/I2CACIS.2019.8825045.

[32] F. Ahmad *et al.*, "Fuzzy fractional PID gain controller for antilock braking system using an electronic wedge brake mechanism," *International Journal of Vehicle Safety*, vol. 10, no. 2, p. 97, 2018, doi: 10.1504/IJVS.2018.094154.

[33] F. Ahmad, M. S. Amri, and Z. Hairi, "Modeling and Validation of Quarter Vehicle

Traction Model," *Applied Mechanics and Materials*, vol. 554, no. 01, pp. 489–493, Jun. 2014, doi: 10.4028/www.scientific.net/AMM.554.489.

[34] Z. Dalimus, "Braking System Modeling and Brake Temperature Response to Repeated Cycle," *Journal of Mechatronics, Electrical Power, and Vehicular Technology*, 2014, doi: 10.14203/j.mev.2014.v5.123-128.

[35] J. C. Gerdes and J. K. Hedrick, "Brake system modeling for simulation and control," *Journal of Dynamic Systems, Measurement, and Control*, vol. 121, no. 3, pp. 296–503, 2008, doi: 10.1115/1.2802501.

[36] Malaysia, "Road Transport Act," *Malaysia*, no. July, pp. 1–158, 1987.

[37] K. Hudha, "Non-Parametric Modelling and Modified Hybrid Skyhook Groundhook Control of Magnetorheological Dampers for Automotive Suspension System," Universiti Teknologi Malaysia, 2005.

[38] D. V Gowda and R. A. C, "Slip Ratio Control of Anti-Lock Braking System with Bang-Bang Controller," *International Journal of Computer Techniques*, vol. 4, no. 1, pp. 97–104, 2017.

[39] A. Ghajari and R. Kazemi, "A New Approach to the Electronic Wedge Brake," *SAE Technical Papers*, vol. 1, 2012, doi: 10.4271/2012-01-1801.

[40] A. Z. Zainordin, Z. Mohamed, and F. Ahmad, "Magnetorheological Fluid: Testing on Automotive Braking System," *International Journal of Automotive and Mechanical Engineering*, vol. 18, no. 1, pp. 8577–8584, 2021, doi: 10.15282/ijame.18.1.2021.16.0651.

[41] S. Navarro Gimenez, J. M. Herrero Dura, F. X. Blasco Ferragud, and R. Simarro Fernandez, "Control-Oriented Modeling of the Cooling Process of a PEMFC-Based μ - CHP System," *IEEE Access*, vol. 7, pp. 95620–95642, 2019, doi: 10.1109/ACCESS.2019.2928632.

[42] A. Kubicek, F. Jopp, B. Breckling, C. Lange, and H. Reuter, "Context-oriented model validation of individual-based models in ecology: A hierarchically structured approach to validate qualitative, compositional and quantitative characteristics," *Ecological Complexity*, vol. 22, pp. 178–191, 2015, doi: 10.1016/j.ecocom.2015.03.005.

[43] E. J. Rykiel, "Testing ecological models: The meaning of validation," *Ecological Modelling*, 1996, doi: 10.1016/0304-3800(95)00152-2.

[44] R. G. Sargent, "Verification and Validation of Simulation Models: An Advanced Tutorial," 2020, doi: DOI: 10.1109/WSC48552.2020.9384052.

Appendix 1. Detail Drawing of CW-EWB

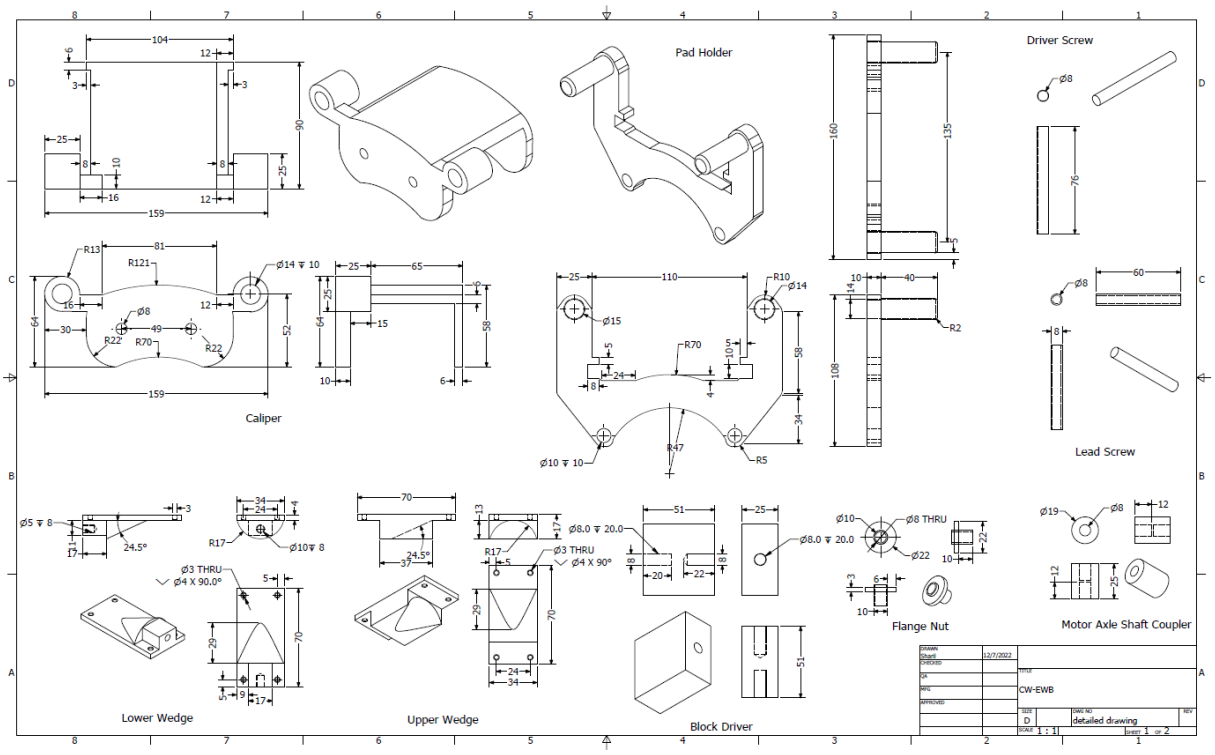

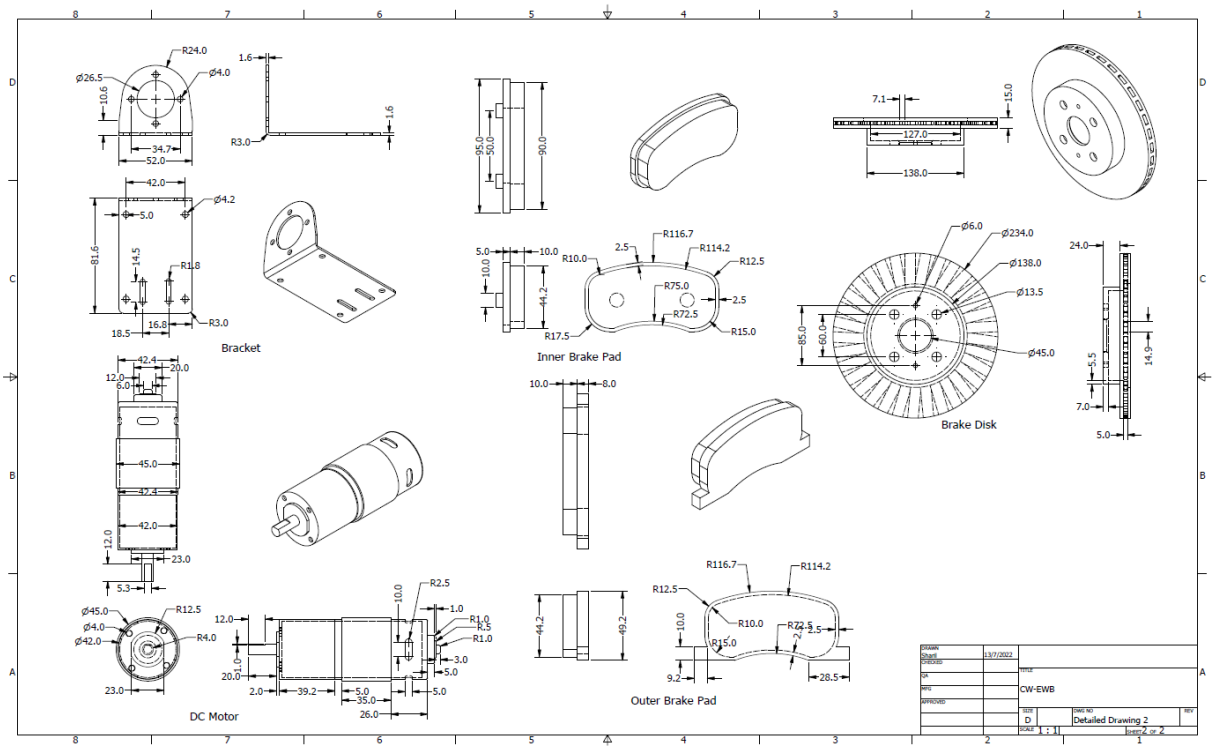

Appendix 2. CW-EWB Model